Membrane Structure of the Human Immunodeficiency Virus gp41 Fusion Domain by Molecular Dynamics Simulation

Shantaram Kamath and Tuck C. Wong
Department of Chemistry, University of Missouri, Columbia, Missouri 65211 USA

ABSTRACT The structures of the16-residue fusion domain (or fusion peptide, FP) of the human immunodeficiency virus gp41 fusion protein, two of its mutants, and a shortened peptide (5–16) were studied by molecular dynamics simulation in an explicit palmitoyloleoylphosphoethanolamine bilayer. The simulations showed that the active wild-type FP inserts into the bilayer ~44° ± 6° with respect to the bilayer normal, whereas the inactive V2E and L9R mutants and the inactive 5 to 16 fragment lie on the bilayer surface. This is the first demonstration by explicit molecular dynamics of the oblique insertion of the fusion domain into lipid bilayers, and provides correlation between the mode of insertion and the fusogenic activity of these peptides. The membrane structure of the wild-type FP is remarkably similar to that of the influenza HA_2 FP as determined by nuclear magnetic resonance and electron spin resistance power saturation. The secondary structures of the wild-type FP and the two inactive mutants are quite similar, indicating that the secondary structure of this fusion domain plays little or no role in affecting the fusogenic activity of the fusion peptide. The insertion of the wild-type FP increases the thickness of the interfacial area of the bilayer by disrupting the hydrocarbon chains and extending the interfacial area toward the head group region, an effect that was not observed in the inactive FPs.

INTRODUCTION

Enveloped viruses such as human immunodeficiency virus (HIV) and influenza virus infect their target cells by a process involving cell-specific binding to the cell membrane followed by fusion of the viral enveloped membrane with cellular membranes (Veronese et al., 1985). Usually only one viral protein is responsible for the actual membrane fusion step. For many viruses, a small segment of the fusion protein usually located at the N terminus of the fusion protein is responsible for the early stage in the membrane fusion process (Chan et al., 1997). This domain is usually referred to as the fusion domain or fusion peptide (FP). The interaction of this segment with membranes has certain membrane perturbing properties (Peisajovich et al., 2000) and can accelerate the rate of liposome fusion in model membrane systems. In the case of HIV, the envelope glycoprotein gp160 of the human immunodeficiency virus type 1 (HIV-1) contains two noncovalently associated subunits, gp120 and gp41 (Veronese et al., 1985). The subunit gp120 contains sites for viral binding to target cells containing CD4 (Lasky et al., 1987) and chemokine receptors (Choe et al., 1996; Doranz et al., 1996; Dragic et al., 1996), whereas the transmembrane subunit, gp41, is responsible for the membrane fusion process (Kowalski et al., 1987). The 16 residues of the gp41 N-terminal fusion domain (AVGIGALFLGFLGAAG) are mostly hydrophobic, and the FP is highly homologous with corresponding domains of other enveloped viruses (Gallaher, 1987). An absolutely conserved five-residue FLGFL sequence at positions 8 to 12 is a prominent motif among the HIV family and was proposed to be essential in fusogenic activities (Pritsker et al., 1999).

Strong evidence coming from mutagenesis studies of intact enveloped proteins as well as from synthetic FPs implicates the role of the FP domain in mediating membrane fusion (Delahunty et al., 1996; Freed et al., 1990, 1992). Mutations with a polar residue in this domain either in intact gp41 fusion protein or in synthetic peptides, such as V2E and L9R, reduce the fusogenic activities drastically (Delahunty et al., 1996; Freed et al., 1992; Mobley et al., 1999).

Polarized attenuated total reflection infrared spectroscopy has been used to determine the orientation of fusion peptides with respect to the membrane surface (Martin et al., 1993, 1996). It was suggested that, based on the correlation of the tilt angle of the inserted FP with respect to the membrane interface and the fusogenic activity of the FP, the oblique insertion of the viral FP is required for fusogenic activities. Inactive FP mutants orient parallel to the membrane surface instead. Whereas Fourier transform infrared is effective in determining the gross orientation of the peptides with respect to the membrane surface, it does not provide detailed structural information or information on the specific interactions between the peptides and the membrane host. There has been no high-resolution structural determination of the gp41 fusion domain in membrane to date. A few nuclear magnetic resonance (NMR) studies provided some useful structural information on the FP/membrane systems. Chang et al. (1997) using solution NMR techniques to study the structure of the 23-mer in model membrane systems (sodium dodecyl sulfate micelles, DMPC, and DPPS vesicles). The 23-mer and its F8W mutant interact with the model membrane by inserting the 1 to 16 hydrophobic segment into the membrane interior as a helix,

Submitted November 7, 2001, and accepted for publication February 13, 2002.

Address reprint requests to Tuck C. Wong, Department of Chemistry, University of Missouri, 123 Chemistry Building, Columbia, MO 65211. Tel.: 573-882-7725; Fax: 573-882-2754; E-mail: wongt@missouri.edu.

0006-3495/02/07/135/09 $2.00

whereas the C-terminal 7-residue segment resided on the membrane-water interface. Similarly, Yang et al. (2001a,b) used solid state NMR to show that the membrane-bound HIV 23-mer FP adopts a β-sheet structure and that the structure distribution is dependent on the lipid composition.

To date, only a few modeling/simulation studies on the interaction of viral fusion peptides with membrane. Hydrophobic moments and hydrophobic index have been used to estimate the interaction of the HIV and other FPs with membrane. Efremov et al. (1999) used Monte Carlo simulation to study the orientation of the influenza hemagglutinin HA_2 (1–20) FP in a lipid bilayer represented by a two-phase slab model. Bechor and Ben-Tal (2001) used molecular dynamics (MD) in an implicit solvent model to study the orientation of the HA_2 FP with respect to the membrane and found that the free energy of the system is lower for the parallel (between the peptide helical axis and the membrane-water interface) orientation than the oblique orientation suggested from experimental results (Luneberg et al., 1995; Zhou et al., 2000). These authors attributed the discrepancy to the neglect of the head group-peptide interactions and peptide-induced membrane deformation in the implicit solvent model. Simulations using explicit bilayer models do include these effects and should render a more realistic and accurate picture of the interactions. In this work, we report the results of an MD study of the HIV-1 wild-type FP (FP-wt), its V2E (FP-V2E) and L9R (FP-L9R) mutants, and a shortened peptide consisting of the 5 to 16 segment [FP-(5–16)] in an explicit palmitoyloleoyl-phosphatidylethanolamine (POPE) lipid bilayer. The V2E and L9R mutants were selected because these point mutations have been shown to suppress gp41 fusion activities (Freed et al., 1990, 1992) and lipid mixing and hemolysis activities of the corresponding synthetic peptides in model liposomes (Kliger et al., 1997; Mobley et al., 1999; Pereira et al., 1995). The shortened (5–16) peptide was chosen for this study because previous work showed that transfection of CD^{4+} HeLa cells with the shortened FP lacking the 1 to 4 N-terminal segment was found to eliminate syncytia formation (Schaal et al., 1995). A previous work showed that the FP can only cause fusion of large unilamellar vesicles when phosphatidylethanolamine (PE) is present and the orientation of the FP with respect to the bilayer surface depends on the presence of PE (Martin et al., 1993). We have thus used the zwitterionic POPE bilayer to investigate the interaction of the fusion peptides with the lipid bilayer.

The explicit MD simulations were able to determine the membrane structures of these fusion peptides that are consistent with experimental determinations to date, to correlate the membrane structure with their fusogenic activities, and to provide insight into the secondary structure of the fusion peptides and the bilayer perturbation upon binding of the active fusion peptides to the bilayer.

MATERIALS AND METHODS

The explicit peptide-POPE bilayer in water was subjected to molecular dynamics simulations and minimizations using CHARMM (Brooks et al., 1983) version 27b1 running on a Cray T3E at the Pittsburgh Supercomputing Center. The energy of the system was expressed by the all atom PARAM-27 force field (MacKerell et al., 1998) that includes phospholipids and TIP3P water potentials. The nonbonded list was generated using a group-based cutoff of 14.0 Å. The van der Waals interactions were smoothly switched from 10.0 to 12.0 Å. The long-range electrostatic interactions were handled by the particle mesh Ewald algorithm (Darden et al., 1993) using a $48 \times 48 \times 81$ grid and a β-spline interpolation of 4^{th} order. FP-wt and FT-(5–16) were constructed in an α-helical conformation. The N terminus was protonated and the C terminus was modeled as a carboxamide. The coordinates for the POPC-bilayer system were obtained from Professor Helmut Heller's laboratory (http://www.lrz-muenchen.de/~heller/membrane/membrane.html), and a bilayer slice of 50×50 Å from the center of the bilayer system was used for simulation. The water from the initial system was deleted and the choline groups were changed to ethanolamine groups and the resulting bilayer was centered in a tetragonal box of dimensions $50 \times 50 \times 84$ $Å^3$. This system was then solvated and equilibrated. The peptide was next inserted into the upper leaflet of the bilayer keeping the helical axis perpendicular to the bilayer surface. The POPE and water molecules overlapping with the peptide were deleted. The final bilayer had 33 and 40 lipid molecules on the upper and lower leaflets of the bilayer, respectively. The SHAKE algorithm (Ryckaert et al., 1977) was used to fix the lengths of bonds involving hydrogen atoms. The Newton's equations of motion were integrated every 2 fs using the leapfrog Verlet algorithm (Verlet, 1967). Periodic boundary conditions were applied to the system to prevent distortions at the boundary of the system as a result of exposure to vacuum. The system was minimized for 2000 cycles using steepest descents to remove bad van der Waals contacts. Following minimizations distance restraints to the hydrogen bonds to maintain the helical nature of the peptide were applied during the heating period and a small portion of the equilibration period after which the restraints were removed. The temperature of the system was maintained at 320 K during the entire data sampling period and was checked every 50 steps and maintained within 3 K of 320 K by velocity scaling. The nonbonded list was updated every 10 steps. A NPT ensemble was used during data sampling. The mass of the Langevin piston (Feller et al., 1998) was set to 500 amu and the collision frequency 25 ps^{-1}. The pressure was maintained by changing the box length in the z direction along the bilayer axis. During this stage the trajectory was sampled every 0.5 ps. The total simulation time was 1.4 ns for FP-wt and 1.1 ns for FP-(5–16), respectively. The two mutants, FP-L9R and FP-V2E, were constructed from the conformation of FP-wt at the end of the 300 ps of the above run by mutating Leu^9 to Arg and Val^2 to Glu, respectively. The simulations were carried out from that point onwards. The simulation strategy was the same as for FP-wt, except that the total simulation length was 800 ps for FP-V2E and 1.3 ns for FP-L9R. The simulation times for FP-(5–16), FP-V2E, and FP-L9R were shorter than that for FP-wt because these peptides got out of the bilayer and became oriented parallel to the bilayer surface in relatively short time. Each of these three simulations was stopped after the peptide moved out of the bilayer and an additional 500-ps simulation was produced for the purpose of sampling the trajectories.

RESULTS

Insertion of the fusion domain

Because the peptides maintained their helical nature during the entire simulation (see Discussion later), the orientation of the peptides was measured by the tilt angle of the helical axis of the peptides with respect to the bilayer normal. The

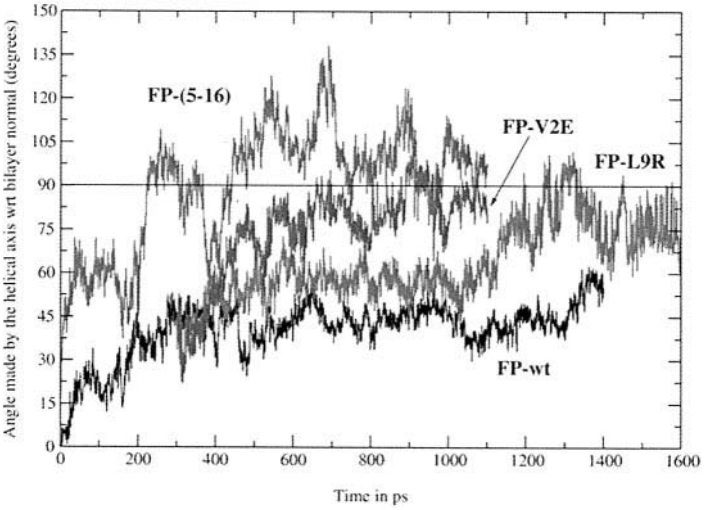

FIGURE 1 Time-evolution of the orientation of the helical axis with respect to the normal to the POPE bilayer for FP-wt, FP-L9R, FP-V2E, and FP-(5–16). The fluctuations of the orientation are much larger for the latter three peptides that have emerged onto the surface of the bilayer.

time evolution of the tilt angle of the helical axis for these four peptides differed significantly. The initial configuration of FP-wt had its helical axis oriented parallel to the bilayer normal (i.e., perpendicular to the bilayer surface). The helical axis slowly tilted during the simulation, reaching an equilibrium orientation of 44° ± 6° with respect to the bilayer normal at ~300 ps (Figs. 1 and 2). The helical axis fluctuated to a limited extent about this average angle throughout the rest of the sampling period. Significant changes in the helical axis orientation from that of FT-wt were seen after the mutations. The mutants FP-V2E and FP-L9R, oriented at 80° ± 8° and 77° ± 10° with respect to the bilayer normal, respectively, after reaching their equilibrium configurations. The shortened peptide FP-(5–16) moved very quickly (in less than 200 ps) out of the bilayer onto the surface, making a tilt angle of 99° ± 13° with the bilayer normal and appeared to have a slight insertion of the C terminus into the lipid bilayer. Substantially increased fluctuations in the orientation occurred after the peptide emerged onto the bilayer surface due to the greater degree of motion of the peptides on the surface of the bilayer, as seen in FP-V2E, FP-L9R, and FP-(5–16) (Fig. 1). This is the first MD work that demonstrated the oblique orientation of the fusogenic gp41 FP (or any other viral FP) with respect to the lipid bilayer. Martin et al. (1996) used attenuated total reflection infrared spectroscopy to study FP-wt, FP-(5–16), and several other variants in PE/phosphatidycholine bilayers. Our present simulation results on the orientation of the FPs with respect to the bilayer surface are in excellent quantitative agreement with those determined in Martin's work for FP-wt and FP-(5–16) (40° ± 5° and 90° ± 5°, respectively).

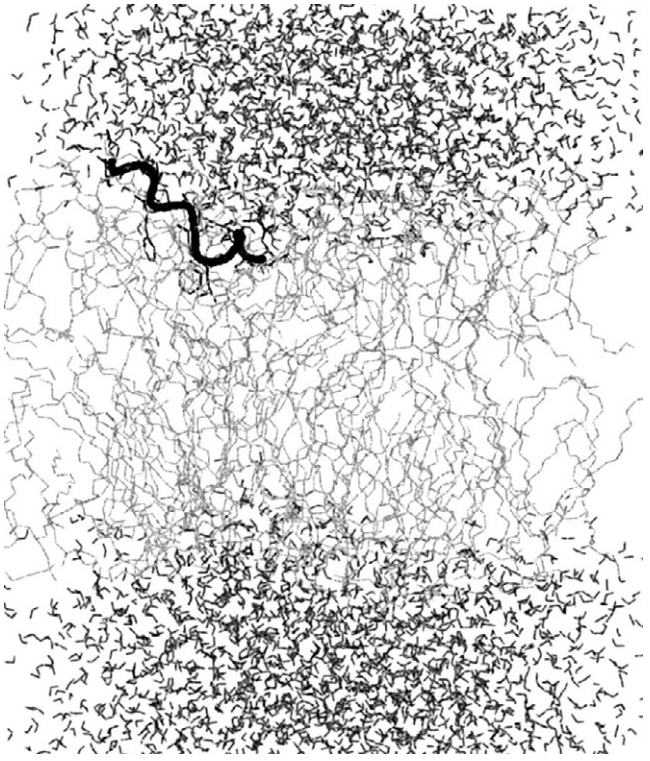

FIGURE 2 Structure of the FP-wt/POPE system after 1.1 ns of MD simulation.

The positions of the side chains and backbones of the various residues in the peptides in the bilayer provide information on the extent of the insertion of the various peptides into the bilayer. In Fig. 3, the locations of the backbone and the side chains (average positions of the heavy atoms on the backbone and the side chain, respectively) of the peptides in the POPE matrix are shown. On the vertical axis the radial distributions (RDF) for the various groups of the lipids are displayed. The interfacial area of the bilayer between the bilayer and water is calculated based on the positions where the hydrocarbon and water densities pass through 10% of their bulk values (MacKerell, 1995). The interfacial area in each system in Fig. 3 is indicated by

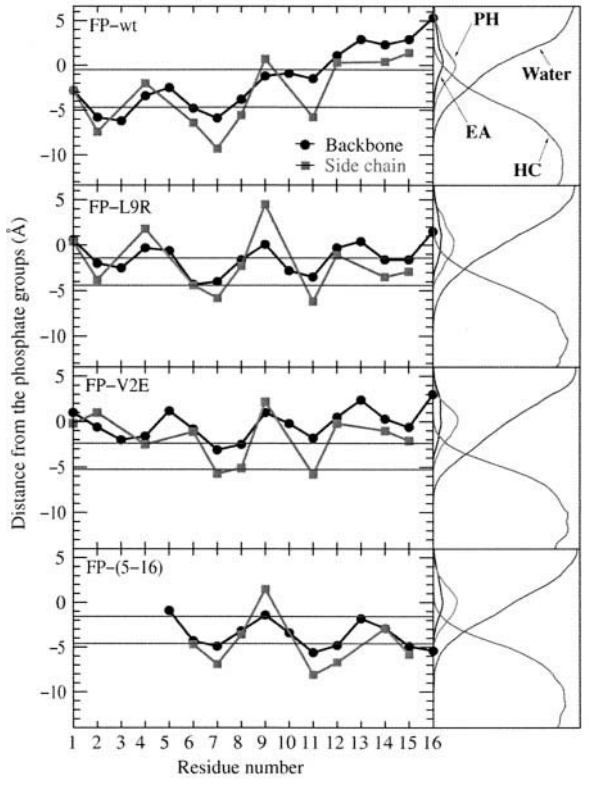

FIGURE 3 Distribution of the peptide backbone and side chains of each residue in FP-wt, FP-L9R, FP-V2E, and FP-(5–16) with respect to the various regions of the POPE bilayer matrix (HC, hydrocarbon; EA, ethanolamine; PH, phosphate). The radial distribution functions for the various groups of the lipid matrix are plotted on the vertical axis. Note that these figures were not drawn to reflect the angle of orientation with respect to the bilayer accurately.

the two horizontal lines. The head group area is the area where the phosphate and ethanolamine groups are distributed and is 2 to 3 Å closer to the aqueous phase than the interfacial area (Fig. 3). FP-wt has its N-terminal segment inserted deeper than the interfacial area whereas the C-terminal segment lies in the head group area. FP-V2E lies entirely in the head group area of the bilayer except for the side chains of Ile^4, Leu^7, Phe^8, and Phe^{11} that penetrate into the interfacial area anchoring the peptide loosely on the surface of the bilayer almost parallel to the bilayer surface. FP-L9R lies deeper with respect to the bilayer than FP-V2E, distributed mostly in the interfacial area with the same side chains as FP-wt interacting with the hydrophobic interior of the bilayer. The location of FP-(5–16) in the bilayer is similar to that of FP-L9R with a slight insertion of the C terminus. Viewing the FPs in a Schiffer-Edmundson helix wheel diagram (Schiffer and Edmundson, 1967), it can be shown that most of the glycines form a strip segregated from the more hydrophobic residues such as Phe, Ile, and Leu (Mobley et al., 1999). This feature provides the amphipathicity that facilitates the interaction with the bilayer with the glycines (with the exception of Gly^3) facing the aqueous phase and the more hydrophobic face of the helix orienting toward the interior of the bilayer.

Introduction of a polar residue into the FP as in FP-V2E and FP-L9R resulted in a reduction of the capacity of the peptide to insert into the lipid bilayer compared with the FP-wt. It appears that the first few N-terminal residues of the FP are most essential in keeping the peptide inserted. The peptide with a polar mutation in this region (FP-V2E) and the peptide lacking this segment entirely [FP-(5–16)] move out of the bilayer quickly (600 and 200 ps, respectively), whereas a polar mutation at the 9th position (FP-L9R), although eventually leading to a surface-binding position, takes a much longer time (1.2 ns) for the peptide to migrate to the bilayer surface.

The membrane structure of the FP-wt is remarkably similar to the structure determined for the influenza HA_2 viral fusion peptide in micelles by NMR and electron spin resistance (ESR) techniques by Zhou et al. (2000) in DOPC unilamellar vesicles and in a recent work by Han et al. (2001) in 4:1 POPC:POPG unilamellar vesicles. In these investigations, the immersion depth of the HA_2 fusion peptide was determined by the ESR power saturation techniques (Altenbach et al., 1994; Macosko et al. 1997). The angle (53° insertion for the HA_2 FP in Han et al., 2001) and the depth of insertion of the N terminus, and the oscillation of the depths of the residues with a periodicity of 3.6 residues are all quite similar in these two FP-membrane systems. The correlation of the depth of insertion (or the tilt angle) of the HIV FP with its activity obtained in this study, i.e., a sufficiently deep insertion (or an oblique orientation) is correlated with fusion activities whereas a lack of peptide insertion reflects inactivity, is also similar to the difference in the insertion pattern of the HA_2 FP at higher (7.4) and lower pH (5) values (67° and 53°, respectively with respect to the bilayer normal). The active form of the HA_2 FP at lower pH displayed a deeper insertion than the inactive high pH form (Han et al., 2001). The explicit MD technique has proved to be a powerful technique in obtaining atomic level information on the membrane structure of the fusion domain of viral proteins and can provide even more detailed information on the structure, interactions, and correlations of structure to activity when combined with experimental techniques such as NMR and ESR power saturation in such studies. The apparent difference between the locations of the depth mapping of this work and those of Zhou et al. (2000) and Han et al. (2001) is due to the fact that the latter studies mapped the location, not of the peptide backbone directly, but of the spin labels attached to each of the backbone segments. The location of the unpaired electron in the spin label is approximately an additional 5 Å further away from the helical axis than the backbone, leading to an apparently larger oscillation in the depth of the positions of the individual segments (Zhou et al., 2000).

TABLE 1 ϕ **and** ψ **values (in dgrees) for the wild-type fusion peptide and nits mutants**

	Phi and psi values*							
	FP-WT		FP-L9R		FP-V2E		FP-(5-16)	
Residue	ϕ	ψ	ϕ	ψ	ϕ	ψ	ϕ	ψ
2	−85 ± 18	132 ± 14	−98 ± 20	156 ± 14	−83 ± 15	149 ± 13	–	–
3	102 ± 22	−13 ± 24	128 ± 29	−58 ± 23	101 ± 19	−30 ± 20	–	–
4	−72 ± 14	−57 ± 10	−66 ± 12	−48 ± 10	−70 ± 14	−46 ± 9	–	–
5	−62 ± 22	−18 ± 36	−64 ± 11	−42 ± 13	−62 ± 11	−44 ± 14	–	–
6	−96 ± 31	−63 ± 13	−92 ± 12	−54 ± 11	−68 ± 12	−51 ± 13	−92 ± 18	−67 ± 21
7	−90 ± 15	−54 ± 12	−85 ± 11	−62 ± 12	−83 ± 12	−60 ± 12	−75 ± 13	−66 ± 14
8	−75 ± 12	−34 ± 12	−72 ± 12	−56 ± 10	−76 ± 13	−50 ± 10	−71 ± 11	−47 ± 10
9	−47 ± 19	−44 ± 16	−70 ± 9	−28 ± 13	−72 ± 8	−26 ± 10	−76 ± 12	−38 ± 20
10	−65 ± 11	−35 ± 12	−66 ± 13	−52 ± 14	−64 ± 11	−35 ± 12	−77 ± 17	−57 ± 15
11	−74 ± 11	−39 ± 9	−69 ± 11	−53 ± 8	−63 ± 10	−49 ± 8	−71 ± 12	−52 ± 12
12	−65 ± 9	−40 ± 10	−68 ± 9	−30 ± 10	−63 ± 9	−39 ± 10	−71 ± 13	−36 ± 23
13	−67 ± 11	−30 ± 15	−71 ± 11	−33 ± 13	−67 ± 11	−32 ± 14	−77 ± 24	−47 ± 21
14	−72 ± 12	−37 ± 12	−75 ± 12	−33 ± 11	−74 ± 12	−40 ± 11	−73 ± 12	−46 ± 13
15	−73 ± 12	−55 ± 17	−71 ± 11	−52 ± 19	−72 ± 12	−55 ± 17	−72 ± 11	−49 ± 18

*Values are reported as mean ± SD.

Secondary structure and conformational transitions

All four FPs studied maintained their helical structure throughout the simulations. By examining the ϕ, ψ angles of each corresponding residues of these peptides, it can be concluded that there is hardly any differences between the secondary structures of the active FP-wt and the inactive FP-V2E, FP-L9R, and FP-(5–16) (Table 1). This result supports the hypothesis that the variation in the secondary structure in the fusion domain plays little or no role in their fusogenic activities. Several FPs (HIV and SIV) and their inactive mutants were found to share the same solution and membrane-bound secondary structures. Thus, the secondary structure of the FPs cannot be a primary parameter in determining their fusogenic activities (Martin et al., 1991, 1994, 1996).

The hydrogen bonding patterns in these four fusion peptides have been analyzed from their MD trajectories. The criteria for defining a hydrogen bond are an average acceptor (oxygen in this case)-hydrogen distance of <2.8 Å and an average O—H—N angle of $>120°$ (Ravishanker et al., 1994). Hydrogen bonding patterns characteristic of an α-helix, i.e., C═O (i)—NH (i + 3) and C═O (i)—NH (i + 4) hydrogen bond are observed through most part of all four of the peptides, indicating an α-helical structure. The i, i + 4 hydrogen bonds are usually the stronger, as judged by the distance between the O and H atoms and the O···H—N angle. The exception is in the region from C═O of Ile^4 to C═O of Leu^7 for FP-wt and from Ile^4 to Ala^6 for FP-L9R in which the i, i + 3 and i, i + 4 hydrogen bonds with the amide protons are missing (or are much weaker) (Table 2). Analysis of the interaction between the C═O oxygen and the N-H proton of the peptide backbone with water and the lipid head groups via the respective RDF showed that the carbonyl oxygen atoms of Gly^5, Ala^6, and Leu^7 are more strongly hydrated by water than others residues in the mid-section of the peptide (e.g., Ile^4, Phe^8, and Phe^{11}) (Fig. 4), even though Ala^6 and Leu^7 are both on the hydrophobic face of the helix facing the interior of the bilayer (Fig. 3). This partially explains the weakening of the hydrogen bonding in the 4 to 6 segment. The strongest hydrogen bonds were found in the segment starting with the FLGFL motif and extending toward the C terminus for FP-wt. For the two mutants, the segment of the strongest hydrogen bonding starts at residue 7. The strength of the hydrogen bonds in the two mutants are practically the same as in FP-wt with the exception of the hydrogen bond between C═O (9) and N—H (13) in FP-L9R, which is weakened compared with corresponding hydrogen bonds in other two FPs due to the L9R mutation (Table 2). For FP-(5–16) the intramolecular hydrogen bonds are uniformly and appreciably weaker than the corresponding hydrogen bonds in FP-wt and the other mutants as judged by the longer O—H distances and smaller O—H—N angles (Table 2). This probably means that the helical structure in FP-(5–16) is not as tight as in the longer peptides, making it less desirable to stay in the hydrophobic part of the bilayer.

Among the three inactive peptides, only FP-L9R showed a significant conformational transition during the simulation period. However, that is not the case for the FP-wt where a significant conformational transition took place twice during the 1.4-ns simulation. The transitions for FP-wt occurred at the ϕ angle of Gly^3, Ala^6, and Leu^9 and ψ angle of Gly^5 leading the peptide to go from a linear to a V-shaped form pivoted at Gly^5. The V-shaped conformation persisted for 200 ps and then the peptide returned to the linear form. Another transition took place later and persisted for only ~30 ps. The lack of hydrogen bonding in the 4 to 7 segment

TABLE 2 Hydrogen bonding patterns of the wild-type fusion peptide and its mutants

H-bond pattern	Bond angles and bond distances*							
	FP-WT		FP-L9R		FP-V2E		FP(5–16)	
	Angle	Distance	Angle	Distance	Angle	Distance	Angle	Distance
2 → 6	–	–	–	–	–	–		
3 → 7	145 ± 16	2.86 ± 1.l0	157 ± 13	2.17 ± 0.4	156 ± 13	2.49 ± 0.7		
4 → 8	–	–			126 ± 21	2.52 ± 0.4		
5 → 9	–	–	–	–	–	–	–	–
6 → 10	–	–	–	–	–	–	121 ± 16	2.84 ± 0.6
7 → 11	–	–	152 ± 17	2.29 ± 0.4	144 ± 16	2.42 ± 0.4	130 ± 24	2.75 ± 0.5
8 → 11	126 ± 16	2.44 ± 0.3	–	–	125 ± 15	2.78 ± 0.4	–	–
8 → 12	159 ± 12	2.11 ± 0.3	152 ± 21	2.29 ± 0.5	159 ± 11	2.56 ± 0.4	–	–
9 → 13	154 ± 14	2.10 ± 0.3	135 ± 17	2.45 ± 0.5	153 ± 14	2.15 ± 0.3	125 ± 23	2.92 ± 0.7
10 → 14	141 ± 18	2.48 ± 0.5	146 ± 16	2.48 ± 0.5	145 ± 16	2.39 ± 0.4	132 ± 21	2.72 ± 0.6
11 → 14	–	–	–	–	123 ± 14	2.76 ± 0.4	–	–
11 → 15	149 ± 16	2.31 ± 0.4	153 ± 15	2.14 ± 0.3	156 ± 14	2.16 ± 0.3	137 ± 24	2.82 ± 0.7
12 → 16	154 ± 21	2.16 ± 0.5	151 ± 19	2.12 ± 0.4	152 ± 23	2.11 ± 0.5	135 ± 25	2.91 ± 1.1

*Bond angle is the O· · ·H-N angle in degrees and the bond distance is the O· · ·H distance in Å. Values are reported as mean ± SD.

in FP-wt may also be explained by the "hinge" structure formed in this segment. The transitions in these dihedral angles occurred simultaneously during the period 200 to 625 ps of the simulation (Fig. 5 *B*) in a concerted fashion, which seemed to facilitate a deeper insertion of the 1 to 5 segment of the peptide into the bilayer (Fig. 5 *A*) during this initial period of the simulation. In contrast, FP-L9R showed transition only in the ϕ angle of Gly^3 (Fig. 5 *D*) after 900 ps of the simulation. Absence of any such concerted transitions at any other residue in FP-L9R resulted in an upward movement (Fig. 5 *C*) of its 1 to 5 segment away from the bilayer core orienting the entire peptide parallel to the bilayer surface. One of the contributing factors to peptide insertion is a transition of ϕ angle at Leu^9 in FP-wt. Leu^9 is part of the conserved FLGFL motif and is also the residue that is mutated in FP-L9R. These transitions also indicate that the presence of glycines in the 1 to 5 segment is important as it provides conformational flexibility and allows the peptide to insert into the bilayer by reorienting itself.

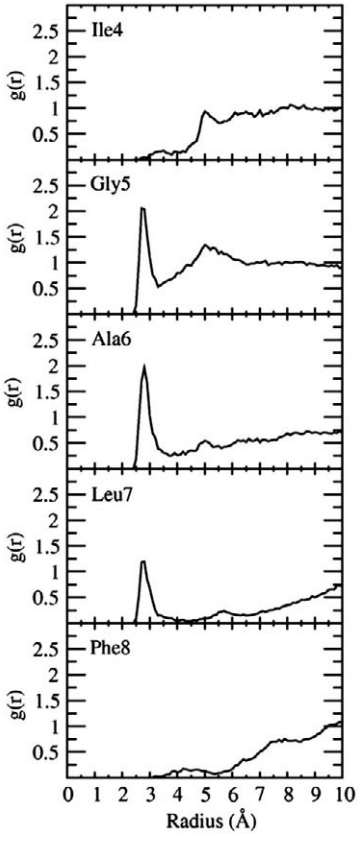

FIGURE 4 Radial distribution functions between the carbonyl oxygen atoms of the peptide bond of respective residues and the oxygen atoms of water for residues Ile^4, Gly^5, Ala^6, Leu^7, and Phe^8 in FP-wt. The hydration of the 5 to 7 segment is substantially higher than the neighboring residues. The C-terminal segment of the peptide is similarly hydrated as the 5 to 7 segment.

Peptide hydration and peptide-head group interactions

As discussed in the previous section the C═O of Gly^5, Ala^6, and Leu^7 of FP-wt showed more significant hydration. The C═O of the C-terminal segment are also more hydrated, indicating greater exposure to the aqueous phase consistent with the insertion pattern and the locations of the C-terminal segment with respect to the membrane-water interface. The hydration of the 4 to 7 segment in FP-V2E and FP-L9R are less conspicuous than in FP-wt, but the C-terminal segment of the mutated peptides is equally hydrated as in FP-wt.

There was surprisingly little interaction between the backbone of the peptides with the phospholipid head groups. Nor was there any significant interactions between the mostly hydrophobic side chains with the lipid head groups. By examining the RDF between the C═O and

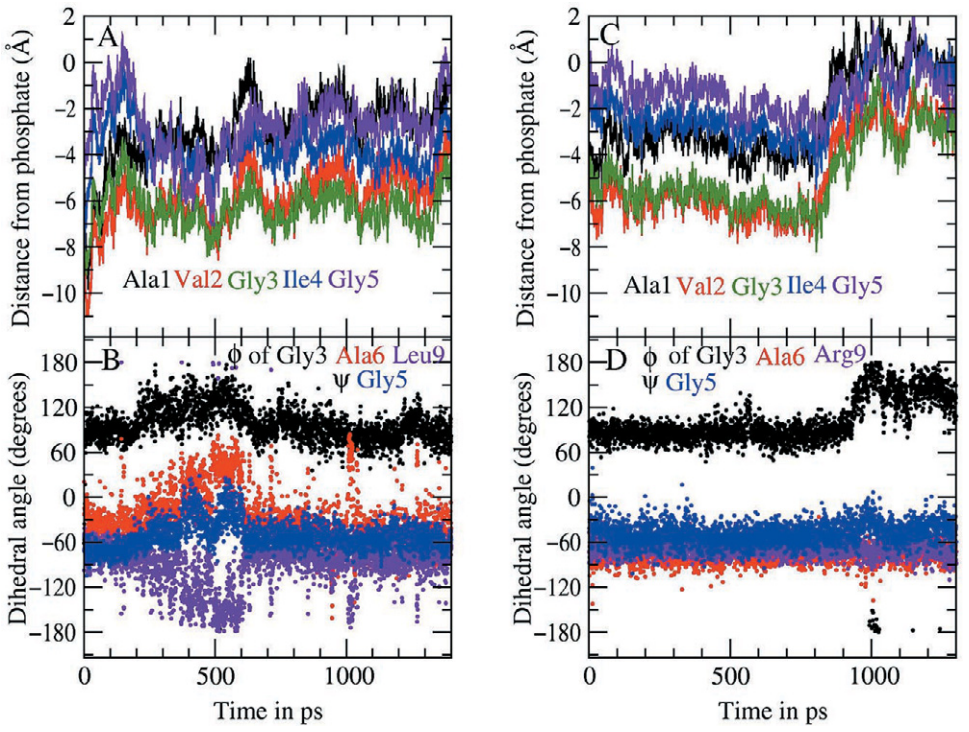

FIGURE 5 Movements of the backbone atoms of residues in the 1 to 5 segment with respect to the phosphate groups of the bilayer during the simulation for FP-wt (*A*) and FP-L9R (*C*) along with the plot of the time evolution of the phi angles of Gly^3, Ala^6, and Leu/Arg^9 and ψ angle of Gly^5 for FP-wt (*B*) and FP-L9R (*D*). The plots for ϕ of Ala^6 and Arg^9 for FP-L9R are not clearly seen due to partial superimposition with ψ of Gly^5.

N—H groups of the backbone and the phosphate and amine groups on the lipids, nonnegligible interactions were found only between the C═O of Ala^{14} of all three 16-residue peptides and of Ala^{15} in FP-V2E and Gly^{16} of FP-L9R with the amine groups in the ethanolamine head groups. Interactions between the amide protons on the backbone of the peptide with the phosphate headgroup are not observed except in FP-(5–16) where there are interactions between the N—H of Ala^2 and Leu^3 with the phosphate head groups. This is in sharp contrast to the case of adrenocorticotropin (1–24) in a DMPC bilayer where more and stronger interactions between the peptide back bone and the head groups were observed (S. Kamath and T. C. Wong, in preparation). This difference probably indicates that the tightly formed helical structure in these fusion peptides shields the backbone of the FP effectively from interacting with the head groups and from being exposed to the hydrophobic environment of the interior of the bilayer. On the other hand, adrenocorticotropin (1–24) does not have nearly as strong intramolecular hydrogen bonding and helical structure as in these FPs, and it possesses many polar/charged side chains. Based on the lack of interactions of either the backbone or the side chains of the gp41 fusion peptides with the lipid head groups and based on the positions of the hydrophobic side chains (e.g., of Val^2, Ala^6, Leu^7, Phe^8, and Phe^{11} in FP-wt), it can be concluded that the interaction of the FPs with the bilayer is primarily through the hydrophobic side chains.

The N-terminal peptide bond in FP-wt is not significantly exposed to the hydrophobic environment because Ala^1 is oriented upward toward the interfacial area, as is the N terminus in the case of the influenza HA_2 FP (Macosko et al., 1997; Zhou et al., 2000) and in the head group area in the case of FP-V2E and FP-L9R (Fig. 3). Instead, the NH_3^+ group of Ala^1 of FP-wt is significantly hydrated and it experiences significant interaction with the phosphate head groups of the POPE (Fig. 6). This indicates that the N terminus is close to the interfacial area and the favorable interaction with the negatively charged head groups provides stabilization of such a configuration. The role of the latter interaction in stabilizing the configuration of the FP in the membrane was also speculated in the study of Macosko et al. (1997) in their study of the influenza HA_2 FP.

Perturbation of the bilayer

The lower leaflet of the bilayer in all four simulations showed an interfacial area thickness of 3.0 ± 0.2 Å, the same as that of an unperturbed POPE bilayer. However, there was an increase of 1.2 Å in thickness of the upper leaflet of the bilayer after the insertion of FP-wt. On the other hand, no detectable change in the thickness of the interfacial area in the upper leaflet of the bilayer was observed for the simulation involving FP-V2E, FP-L9R, and FP-(5–16). There is no indication of an increase in water penetration into the bilayer in the FP-wt case. Therefore, the increase in the length of the interfacial area is not directly correlated with increased water penetration into the bilayer due to the binding of FP-wt. Instead, the disruption of the

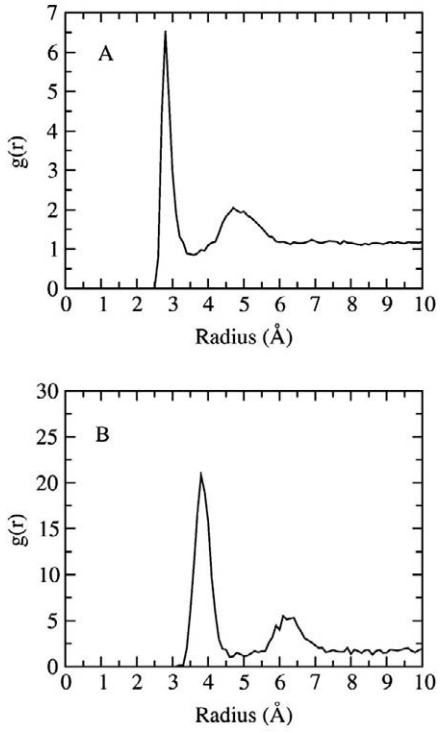

FIGURE 6 RDF between the protonated N-terminal nitrogen and (*A*) the oxygen atoms of water, and (*B*) the phosphorus atoms of the phosphate groups in the POPE head groups, in FP-wt showing strong peaks indicative of significant hydration, and interaction with the phosphate.

bilayer by the FP-wt appears to be manifested in the extension of the distribution of the lipid chains toward the location of the phosphate head groups. Therefore, the location where the lipid density passes through 10% of its bulk value is closer to the head group by ~1.2 Å. This indicates that the oblique insertion of FP-wt disrupts the organization of lipid molecules and increases the disorientation of the lipids and the fluidity of the membrane at the point of insertion by increasing the length of the interfacial area. To observe whether this is the first step preceding the development of a negative curvature and the subsequent fusion process probably requires much longer simulation time, however.

CONCLUSIONS

This work is the first demonstration by explicit MD of the oblique insertion of the active HIV gp41 fusion domain into lipid bilayers and provides correlation between the mode of insertion and the fusogenic activity of these peptides. The results are in excellent agreement with the orientational information obtained from Fourier transform infrared. The membrane structure of the wild-type FP is remarkably similar to that of the influenza HA_2 FP as determined by NMR and ESR techniques. The secondary structures of the wild-type FP and the two inactive mutants are quite similar, indicating that the secondary structure of this fusion domain plays little or no role in affecting the fusogenic activity of the fusion peptide. The insertion of the wild-type FP increases the length of the interfacial area of the bilayer by disrupting the organization of the hydrocarbon chains and extending the interfacial area toward the head group region, an effect that was not observed in the inactive FPs. The combination of explicit MD simulation with experimental techniques such as NMR and ESR power saturation should provide accurate and detailed structural information of the HIV and other fusion peptides in membranes. More importantly, it can provide interpretation of molecular phenomena that may be inaccessible to experimental studies.

Support by the Petroleum Research Fund, administered by the American Chemical Society (35495-AC7), and the Pittsburgh Supercomputing Center are gratefully acknowledged.

REFERENCES

Altenbach, C., D. A. Greenhalgh, H. G. Khorana, and W. L. Hubbell. 1994. A collision gradient method to determine the immersion depth of nitroxides in lipid bilayers: application to spin-labeled mutants of bacteriorhodopsin. *Proc. Natl. Acad. Sci. U. S. A.* 91:1667–1671.

Bechor, D., and N. Ben-Tal. 2001. Implicit solvent model studies of the interactions of the influenza hemagglutinin fusion peptide with lipid bilayers. *Biophys. J.* 80:643–655.

Brooks, B. R., R. E. Bruccoleri, B. D. Olofson, D. J. States, S. Swaminathan, and M. Karplus. 1983. CHARMM: a program for macromolecular energy minimization and dynamics calculations. *J. Comput. Chem*. 4:187–217.

Chan, D. C., D. Fass, J. M. Berger, and P. S. Kim. 1997. Core structure of gp41 from the HIV envelope glycoprotein. *Cell.* 89:263–273.

Chang, D. K., S. F. Cheng, and W. J. Chien. 1997. The amino-terminal fusion domain peptide of human immunodeficiency virus type 1 gp41 inserts into the sodium dodecylsulfate micelle primarily as a helix with a conserved glycine at the micelle-water *Interface. J. Virol.* 71: 6593–6602.

Choe, H., M. Farzan, Y. Sun, N. Sullivan, B. Rollins, P. D. Ponath, L. J. Wu, C. R. Mackay, G. LaRosa, W. Newman, N. Gerard, C. Gerard, and J. Sodroski. 1996. The beta-chemokine receptors CCR3 and CCR5 facilitate infection by primary HIV-1 isolates. *Cell.* 85:1135–1148.

Darden, T., D. York, and L. Pederson. 1993. Particle mesh Ewald: an Nlog(N) method for Ewald sums in large systems. *J. Chem. Phys.* 98:10089–10092.

Delahunty, M. D., I. Rhee, E. O. Freed, and J. S. Bonifacino. 1996. Mutational analysis of the fusion peptide of the human immunodeficiency virus type 1: identification of critical glycine residues. *Virology.* 218:94–102.

Doranz, B. J., J. Rucker, Y. J. Yi, R. J. Smyth, M. Samson, S. C. Peiper, M. Parmentier, R. G. Collman, and R. W. Doms. 1996. A dual-tropic primary HIV-1 isolate that uses fusin and the beta-chemokine receptors CKR-5, CKR-3, and CKR-2b as fusion cofactors. *Cell.* 85:1149–1158.

Dragic, T., V. Litwin, G. P. Allaway, S. R. Martin, Y. X. Huang, K. A. Nagashima, C. Cayanan, P. J. Maddon, R. A. Koup, J. P. Moore, and W. A. Paxton. 1996. HIV-1 entry into CD4(+) cells is mediated by the chemokine receptor CC-CKR-5. *Nature.* 381:667–673.

Efremov, R. G., D. E. Nolde, P. E. Volysky, A. A. Chernyavsky, P. V. Dubovskii, and A. S. Arseniev. 1999. Factor important for fusogenic activity of peptides: molecular modeling study of analogs of fusion peptide of influenza virus hemagglutinin. *FEBS Lett.* 462:205–210.

Feller, S. E., Y. Zhang, R. W. Pastor, and B. R. Brooks. 1998. Constant pressure molecular dynamics simulation: the langevin piston method. *J. Chem. Phys.* 103:4613–4621.

Freed, E. O., E. L. Delwart, G. L. Buchschacher, and A. T. Panganiban. 1992. A mutation in the human immunodeficiency virus type 1 transmembrane glycoprotein gp41 dominantly interferes with fusion and infectivity. *Proc. Natl. Acad. Sci. U. S. A.* 89:70–74.

Freed, E. O., D. J. Myers, and R. Risser. 1990. Characterization of the fusion domain of the human immunodeficiency virus type 1 envelope glycoprotein gp41. *Proc. Natl. Acad. Sci. U. S. A.* 87:4650–4654.

Gallaher, W. H. 1987. Detection of a fusion peptide sequence in the transmembrane protein of human immunodeficiency virus. *Cell.* 50: 327–328.

Han, X., J. Bushweller, D. Cafiso, and L. Tamm. 2001. Membrane structure and fusion-triggering conformational change of the fusion domain from influenza hemagglutinin. *Nat. Struct. Biol.* 8:715–720.

Kliger, Y., A. Aharoni, D. Rapaport, P. Jones, R. Blumenthal, and Y. Shai. 1997. Fusion peptides derived from the HIV Type 1 glycoprotein 41 associated within phospholipid membranes and inhibit cell-cell fusion. *J. Biol. Chem.* 272:13496–13505.

Kowalski, M., J. Potz, L. Basiripour, T. Dorfman, W. C. Goh, E. Terweilliger, A. Dayton, C. Rosen, W. Haseltine, and J. Sodroski. 1987. Functional regions of the envelope glycoprotein of human immunodeficiency virus type 1. *Science.* 237:1351–1355.

Lasky, A. L., G. Nakamura, D. H. Smith, C. Fennie, C. Shimasaki, E. Patzer, P. Berman, T. Gregory, and D. J. Capon. 1987. Delineation of a region of the human immunodeficiency virus type 1 gp120 glycoprotein critical for interaction with the CD4 receptor. *Cell.* 50:975–985.

Luneberg, J., I. Martin, F. Nubler, J. M. Ruysschaert, and A. Hermann. 1995. Structure and topology of the influenza-virus fusion peptide in lipid bilayers. *J. Biol. Chem.* 270:27606–27614.

MacKerell, A. D. 1995. Molecular dynamics simulation analysis of a sodium dodecylsulfate micelle in aqueous solution: decreased fluidity of the micelle hydrocarbon interior. *J. Phys. Chem.* 99:1846–1854.

MacKerell, Jr., A. D., D. Bashford, M. Bellott, R. L. Dunbrack, Jr., J. D. Evanseck, M. J. Field, S. Fischer, J. Gao, H. Guo, S. Ha, D. Joseph-McCarthy, L. Kuchnir, K. Kuczera, F. T. K. Lau, C. Mattos, S. Michnick, T. Ngo, D. T. Nguyen, B. Prodhom, W. E. Reiher, I. I. I., B. Roux, M. Schlenkrich, J. C. Smith, R. Stote, J. Straub, M. Watanabe, J. Wiorkiewicz-Kuczera, D. Yin, and D. M. J. Karplus. 1998. All-atom empirical potential for molecular modeling and dynamics studies of proteins. *J. Phys. Chem. B.* 102:3586–3616.

Macosko, J. C., C. H. Kim, and Y. K. Shin. 1997. The membrane topology of the fusion peptide region of influenza hemagglutinin determined by spin-labeling EPR. *J. Mol. Biol.* 267:1139–1148.

Martin, I., Q. F. Defrise, V. Mandieau, N. M. Nielsen, T. Seermark, A. Burny, R. Brasseur, J. M. Ruysschaert, and M. Vandenbranden. 1991. Fusogenic activities of SIV (Simian Immunodeficiency Virus) peptides located in the gp32 NH_2 terminal domain. *Biochem. Biophys. Res. Commun.* 175:872–879.

Martin, I., F. Defrise-Quertain, E. Decroly, M. Vandenbranden, R. Brasseur, and J. M. Ruysschaert. 1993. Orientation and structure of the NH_2-terminal HIV-1 gp41 peptide in fused and aggregated liposomes. *Biochim. Biophys. Acta.* 1145:124–133.

Martin, I., M. C. Dubois, F. Defrise-Quertain, T. Saermark, A. Burny, R. Brasseur, and J. M. Ruysschaert. 1994. Correlation between fusogenicity of synthetic modified peptides corresponding to the N-terminal extremity of simian immunodeficiency virus gp32 and their mode of insertion into the lipid bilayer: an infrared spectroscopy study. *J. Virol.* 68: 1139–1148.

Martin, I., H. Schaal, A. Scheid, and J. M. Ruysschaert. 1996. Lipid membrane fusion induced by the human immunodeficiency virus type 1 gp41 N-terminal extremity is determined by its orientation in the lipid bilayer. *J. Virol.* 70:298–304.

Mobley, P. W., A. J. Waring, M. A. Sherman, and L. M. Gordon. 1999. Membrane interactions of the synthetic N-terminal peptide of HIV-1 gp41 and its structural analogues. *Biochim. Biophys. Acta.* 1418:1–18.

Peisajovich, S. G., R. F. Epand, M. Pritsker, Y. Shai, and R. M. Epand. 2000. The polar region consecutive to the HIV fusion peptide participates in membrane fusion. *Biochemistry.* 39:1826–1833.

Pereira, F. B., F. M. Goni, and J. L. Nieva. 1995. Liposome destabilization induced by the HIV-1 fusion peptide: effect of a single amino acid substitution. *FEBS Lett.* 362:243–246.

Pritsker, M., J. Rucker, T. L. Hoffman, R. W. Doms, and Y. Shai. 1999. Effect of nonpolar substitutions of the conserved Phe11 in the fusion peptide of HIV-1 gp41 on its function, structure, and organization in membranes. *Biochemistry.* 38:11359–11371.

Ravishanker, G., S. Vijaykumar, and D. L. Beveridge. 1994. STRIPS: an algorithm for generating two-dimensional hydrogen-bond topology diagrams for proteins. *In* Modeling the Hydrogen Bond. American Chemical Society, Washington, DC. 209–219.

Ryckaert, J. P., G. Cicotti, and H. J. C. Berendsen. 1977. Numerical integration of the Cartesian equations of motion of a system with constraints: molecular dynamics of *n*-alkanes. *J. Comput. Phys.* 23: 327–341.

Schaal, H., M. Klein, P. Gerhmann, O. Adams, and A. Scheid. 1995. Requirement of N-terminal amino acid residues of gp41 for human immunodeficiency virus type 1-mediated cell fusion. *J. Virol.* 69: 3308–3314.

Schiffer, M., and A. B. Edmundson. 1967. Use of helical wheels to represent the structures of proteins and to identify segments with helical potential. *Biophys. J.* 7:121–135.

Verlet, L. 1967. Computer "experiments" on classical fluids: I. Thermodynamical properties of Lennard-Jones molecules. *Phys. Rev.* 159: 98–103.

Veronese, F. D., A. L. DeVico, T. D. Copeland, S. Oroszlan, R. C. Gallo, and M. G. Sarngadharan. 1985. Characterization of gp41 as the transmembrane protein coded by the HTLV/LAV envelope gene. *Science.* 229:1402–1405.

Yang, J., C. M. Gabrys, and D. P. Weliky. 2001a. Solid-state nuclear magnetic resonance evidence for an extended β strand conformation of the membrane-bound HIV-1 fusion peptide. *Biochemistry.* 40: 8126–8137.

Yang, J., P. D. Parkanzky, B. D. Khunte, C. G. Canlas, R. Yang, C. M. Gabrys, and D. P. Weliky. 2001b. Solid-state NMR measurements of conformation and conformational distributions in the membrane-bound HIV-1 fusion peptide. *J. Mol. Graphics Modell.* 19:129–135.

Zhou, Z., J. C. Makosko, D. W. Hughes, B. G. Sayer, J. Hawes, and R. M. Epand. 2000. ^{15}N NMR study of the ionization properties of the influenza virus fusion peptide in zwitterionic phospholipid dispersions. *Biophys. J.* 78:2418–2425.